ADVANCED FUNCTIONAL MATERIALS
www.afm-journal.de

# Central Molecular Stacking Regulator Boosts the Efficiency of Organic Solar Cells

*Saisai Liu, Zheng Xu, Ziqi Ma, Wenkai Zhao, Wendi Shi, Guanghui Li, Zhaoyang Yao,* Yaxiao Guo, Guankui Long, Xiangjian Wan, Chenxi Li, and Yongsheng Chen**

**Central unit engineering in non-fullerene acceptors (NFAs) plays a pivotal role in regulating molecular stacking, and further greatly affects the power conversion efficiency (PCE) of organic solar cells (OSCs). A high-efficiency NFA of CS4 is developed in this work, with a sulfur-bridged and chlorinated phenyl group on the central unit as a molecular stacking regulator. Detailed analyses reveal that CS4 exhibits tighter molecular packing, more balanced charge mobility, superior phase separation, and reduced energetic disorder compared to its counterpart, CH3. As a result, a notable efficiency of 18.57% is observed in the D18:CS4-based binary OSC, much higher than 17.81% for that of CH3. Moreover, D18:CS4:BTP-eC9-based ternary device renders a champion PCE of 20.16%. D18:CS4 and ternary devices exhibit enhanced stability over D18:CH3. Under the pressure of 65 °C, $T_{80}$ lifetimes are 1200 h for D18:CS4 and 2500 h for D18:CS4:BTP-eC9-based ternary device. Under continuous light illumination, $T_{80}$ reaches 550 and 710 h, respectively. This study demonstrates an effective strategy to boost high-performance OSCs through precise design of central molecular stacking regulator.**

## 1. Introduction

Organic solar cells (OSCs) represent a viable alternative in third-generation photovoltaics, stimulating considerable research and commercial interest because of their key characteristics: light weight, mechanical flexibility, semi-transparency, and the ability to be processed from solution.[1–10] To advance the commercialization of OSCs, decades of research have focused on both material innovation and device optimization.[11–23] Nowadays, OSCs have achieved remarkable power conversion efficiencies (PCEs) exceeding 20%.[24–31] Nonetheless, even with these advancements, the photovoltaic efficiency of current OSCs remains inferior to that of silicon and perovskite solar cells,[32–34] which could easily surpass 26% PCE. The observed variation originates from the innate flexibility of organic compounds' molecular frameworks and their ensuing loose organization, which is stabilized by weak van der Waals forces instead of strong covalent bonds. These unfavorable molecular packing behaviors usually result in the larger molecular packing disorders and weaker intermolecular action, which further go against the efficient exciton diffusion, dissociation and transport of charge carriers in the active layer of OSCs.[35,36] Therefore, the precise regulation of molecular stacking and active layer morphology is crucially important yet remains greatly challenging.

In this work, a sulfur-bridged and chlorinated phenyl group on the central unit was explored as a molecular stacking regulator, affording a high-efficiency NFA of CS4 (**Figure 1a**). Note that CS4 exhibits a highly ordered molecular arrangement alongside significantly enhanced electronic properties relative to its counterpart, CH3. These favorable properties promote the stronger intermolecular interaction, better crystallinity and reduced energetic disorder of CS4 films. Consequently, the D18:CS4-based binary OSC achieves an efficiency of 18.57%, significantly higher than that of 17.81% for that of CH3. Moreover, D18:CS4:BTP-eC9-based ternary device renders a champion PCE of 20.16%. What's more, devices based on D18:CS4 and ternary organic solar cells exhibit significantly enhanced operational stability compared to D18:CH3-based ones. Under the pressure of 65 °C, the D18:CS4-based device achieved a $T_{80}$ lifetime of 1200 h, which was extended to 2500 h for the D18:CS4:BTP-eC9 ternary device. Under continuous illumination, the $T_{80}$ lifetimes reached 550 and 710 h, respectively. By designing sulfur-bridged central units with halogen modification as a molecular stacking regulator, this

S. Liu, Z. Xu, Z. Ma, W. Shi, G. Li, Z. Yao, X. Wan, C. Li, Y. Chen
State Key Laboratory and Institute of Elemento-Organic Chemistry
The Centre of Nanoscale Science and Technology and Key Laboratory of Functional Polymer Materials
Renewable Energy Conversion and Storage Center (RECAST)
Frontiers Science Center for New Organic Matter
College of Chemistry
Nankai University
Tianjin 300071, China
E-mail: zyao@nankai.edu.cn; yschen99@nankai.edu.cn

W. Zhao, G. Long
School of Materials Science and Engineering
National Institute for Advanced Materials
Renewable Energy Conversion and Storage Center (RECAST)
Nankai University
Tianjin 300350, China

Y. Guo
State Key Laboratory of Separation Membranes and Membrane Processes
School of Chemistry, Tiangong University
Tianjin 300387, China

The ORCID identification number(s) for the author(s) of this article can be found under https://doi.org/10.1002/adfm.202525577

**DOI: 10.1002/adfm.202525577**

 

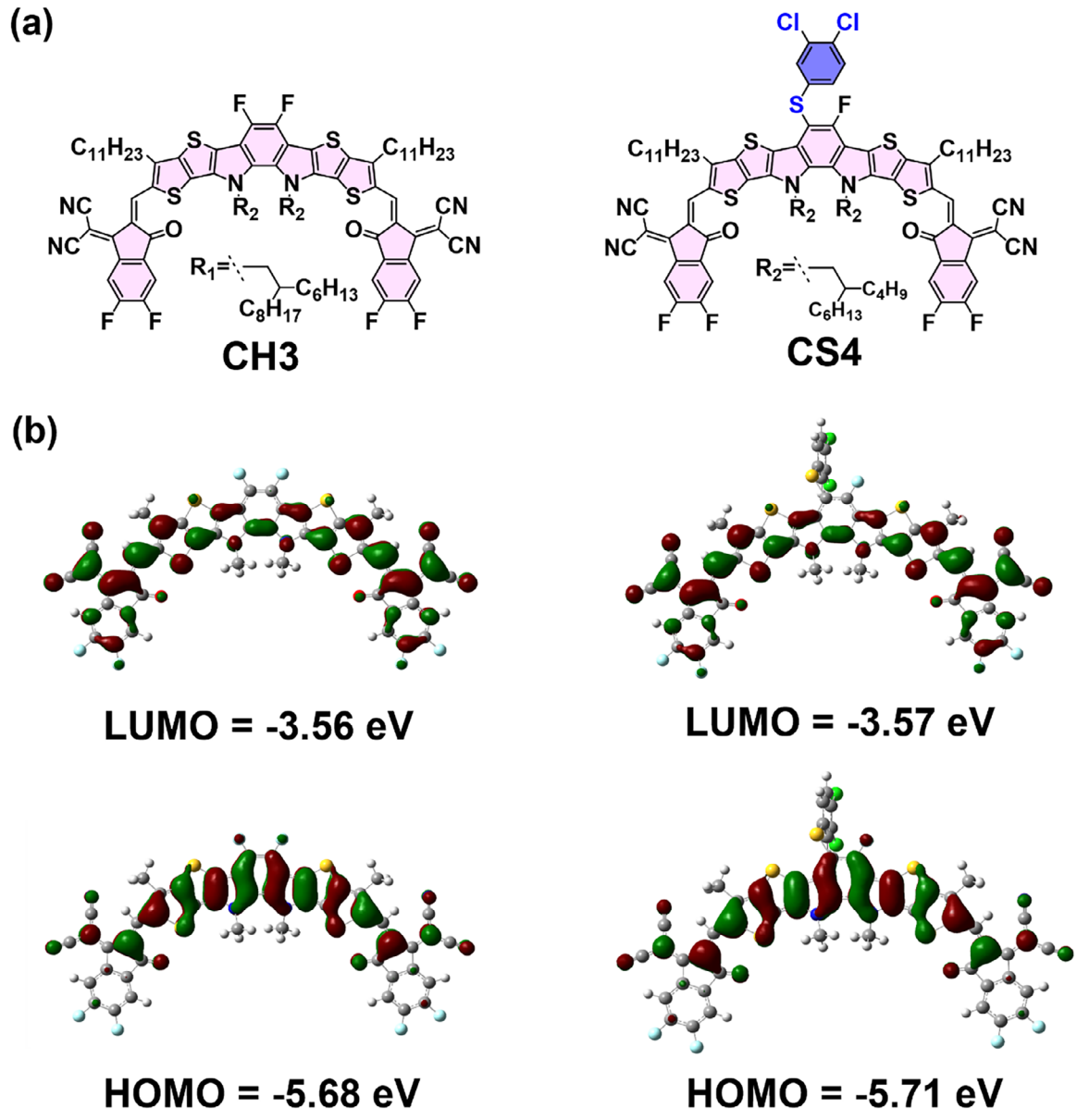


**Figure 1.** a) Molecular structures of CH3 and CS4. b) Molecular frontier orbital (HOMO/LUMO) distributions and energy levels.

study provides an effective strategy to boost high-performance OSCs.

## 2. Results and Discussions

As shown in Figure S1 (Supporting Information), a clear acceptor-donor-acceptor (A-D-A) configuration could be maintained in CS4 after implementation of a sulfur-bridged phenyl group on the central unit, revealed by the distinct peak-valley-peak patterns of frontier orbital charge density difference (ΔQ) plots.[37] However, the dipole moment of CS4 markedly increases to 2.05 Debye compared to that of 1.76 Debye for CH3 (Figure S2, Supporting Information).[38,39] This pronounced A-D-A character and enlarged dipole moment with similar backbones are beneficial for superior molecular packings.[40] For both molecules (CH3 and CS4), the electron density of the lowest unoccupied molecular orbitals (LUMOs) is predominantly located on the cyano groups of the end-cap units. In contrast, the highest occupied molecular orbitals (HOMOs) and LUMOs both exhibit significant spatial overlap on the central S, N-heteroacene core (Figure 1b). It is interesting that the sulfur-bridged phenyl group is perpendicular to S, N-heteroacene and without HOMO distributions. This manifests that the additional phenyl group on the center mainly works as a molecular stacking regulator and has few effects on frontier molecular orbitals. Therefore, CH3 and CS4 possess similar HOMO and LUMO energy levels and bandgaps predicated by density functional theory (DFT) calculations.

The CH3 was synthesized according to the procedures reported by our group and Ding et al.[41–43] Scheme S1

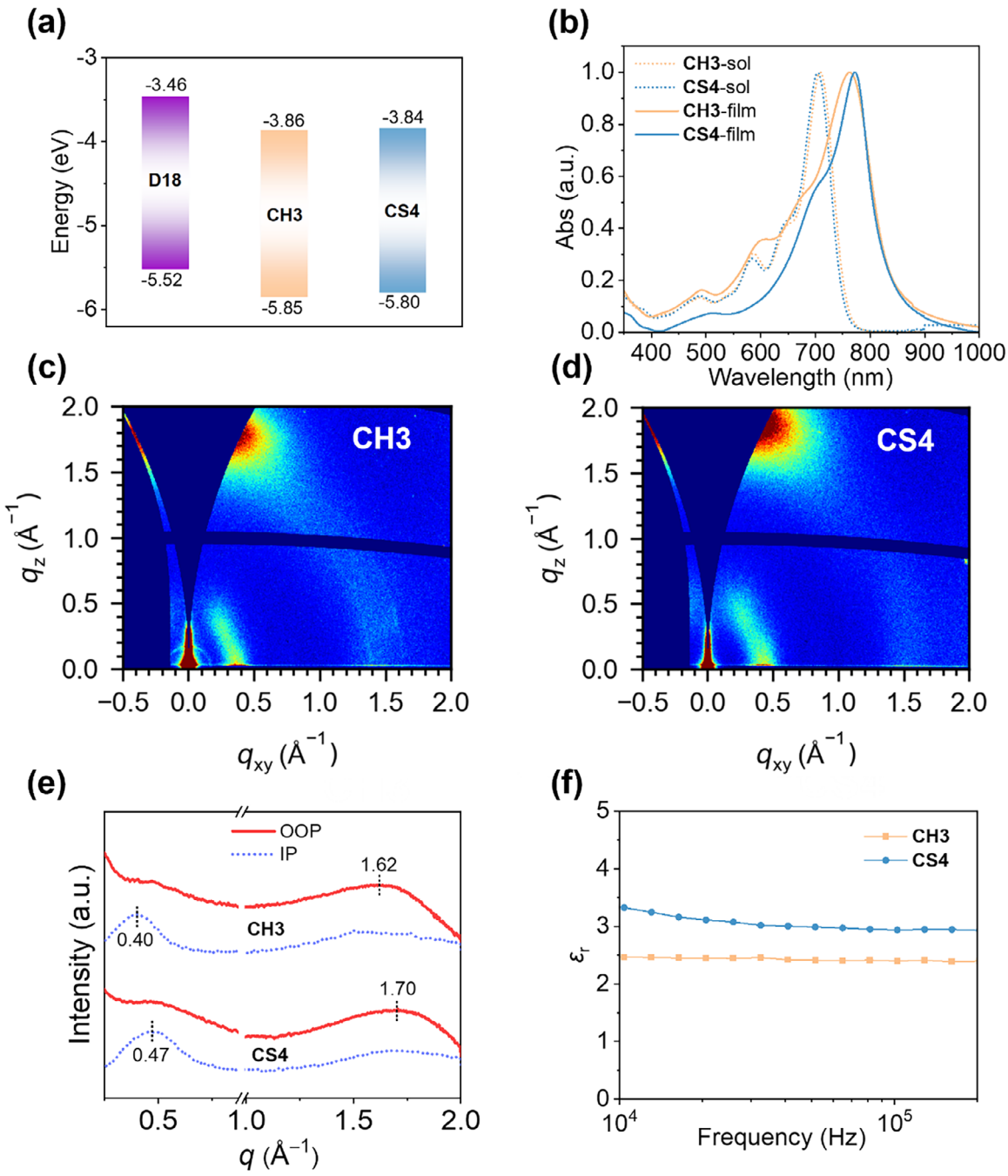


**Figure 2.** a) Energy levels evaluated by cyclic voltammetry (CV). b) Solution-state and film-state normalized UV–vis absorption spectra of two NFAs c, d) GIWAXS images of CH3, CS4-based neat films. e) Line-cut profiles of 2D GIWAXS patterns of CH3 and CS4 neat films. f) $\epsilon_r$ response of CH3 and CS4 neat films at different frequency.

(Supporting Information) outlines the synthesis of the CS4 acceptor. The initial step involved a base-mediated reaction between catechol and compound 1, yielding intermediates compound 2. Subsequent functionalization of compound 2 proceeded via a sequence comprising Cadogan cyclization, alkylation and Vilsmeier reactions. This multi-step transformation furnished compound 3 in a modest yield. Finally, Knoevenagel condensation of compound 3 with 2-(5,6-difluoro-3-oxo-2,3-dihydro-1H-inden-1-ylidene)malononitrile afforded the target molecule of CS4 with an excellent yield of 89%.

The energy levels of CH3 and CS4 were further roughly estimated by electrochemical cyclic voltammetry (Figure S3, Supporting Information). As shown in **Figure** 2a and Table S1 (Supporting Information), the energy levels of LUMO/HOMO were −3.86/−5.85 eV and −3.84/−5.80 eV for CH3 and CS4, respectively. Note that the varying tendency of energy levels derived

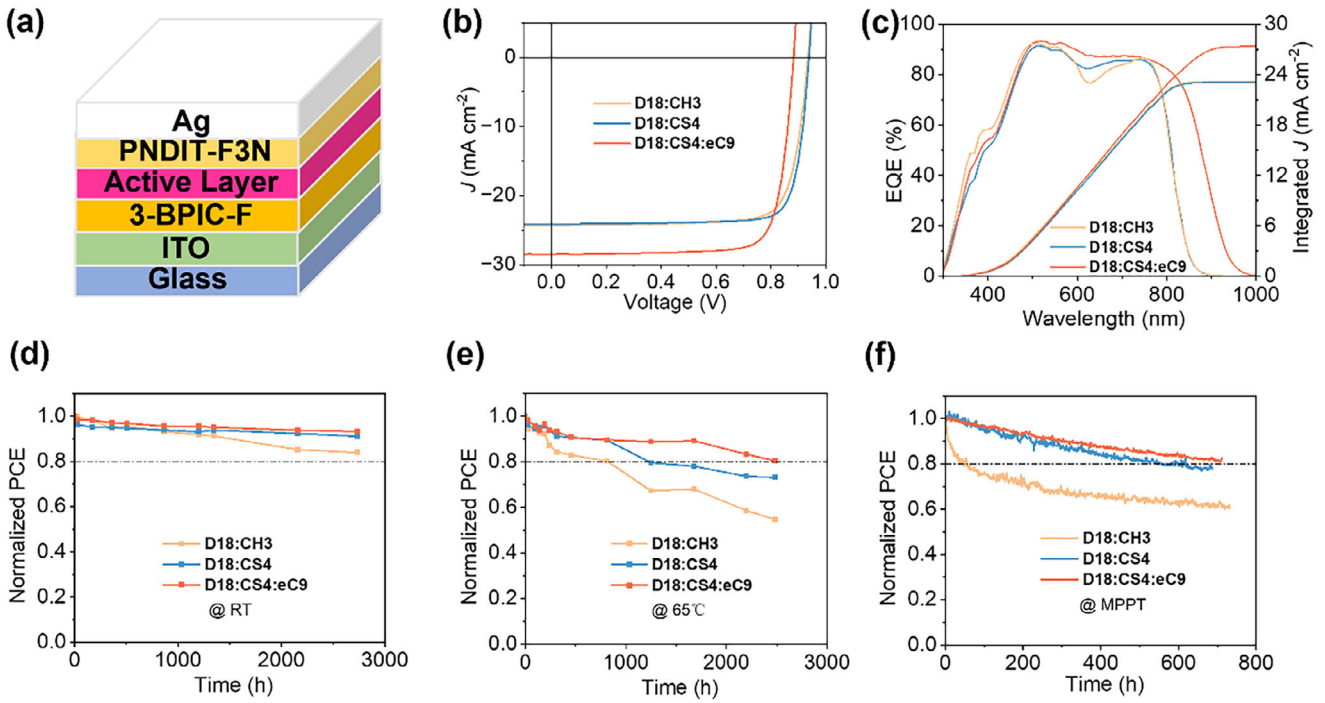


**Figure 3.** a) Device architecture schematics. b) Current density–voltage (*J*–*V*) characteristics of the OSCs. c) EQE spectra. d) Storage stability of optimized devices in the nitrogen-filled glovebox. e) Normalized PCEs of optimized devices under continuous annealing at 65 °C. f) Operational stability test at MPP tracking with continuous illumination (AM 1.5G, 100 mW $cm^{-2}$) at 25 °C in $N_2$ atmosphere.

from CV (solid films) is contradictory to DFT predictions (single molecules). This may be caused by the quite different molecular aggregation behaviors. As a consequence, CS4 shows the slightly blue-shifted maximum absorption peak (704 nm) in diluted chloroform solution, whereas an obviously red shifted one (772 nm) in solid films, compared to that of 710 nm in solution and 763 nm in films for CH3 (Figure 2b; Table S2, Supporting Information). Encouragingly, CS4 exhibited a large redshift of 68 nm when transforming from solutions into films and the smaller peak width at half height compared to CH3. These results indicate that the sulfur-bridged phenyl group on the central unit could exert positive effects on intermolecular $\pi$-$\pi$ stacking of CS4. We then employed grazing-incidence wide-angle X-ray scattering (GIWAXS) to characterize and contrast the molecular packing order, particularly the $\pi$-$\pi$ stacking distance and orientation, in the CH3 and CS4 films (Figure 2c–e; Table S3, Supporting Information).[44] Both the dominant face-on orientation could be observed for CH3 and CS4 neat films, which is critical for efficient out-of-plane (OOP) charge transport.[45] Among them, the OOP (010) $\pi$–$\pi$ diffraction peaks appear at 1.62 $Å^{-1}$ for CH3 and 1.70 $Å^{-1}$ for CS4, corresponding to the $\pi$–$\pi$ stacking distances of 3.88 and 3.69 Å, respectively. The reduction in $\pi$–$\pi$ stacking distance for CS4 signifies the tighter $\pi$-orbital overlap. Moreover, CS4 also indicated the slightly enlarged crystal coherence length (CCL) of 12.70 Å compared to CH3 (9.21 Å) in the (010) direction, suggesting the more ordered molecular packing of CS4. Actually, the decreased $\pi$-$\pi$ stacking distance and enlarged CCL for CS4 are a bit against common sense that the introduction of bulky groups on central units will destroy the compact molecular packings. What's more, we measured the electron mobility of the pure acceptor films (Figure S4, Supporting Information) and found that the electron mobility of CS4 ($2.05 \times 10^{-4}$ $cm^2$ $V^{-1}$ $S^{-1}$) is higher than that of CH3 ($1.17 \times 10^{-4}$ $cm^2$ $V^{-1}$ $S^{-1}$), which is consistent with the more compact and ordered molecular packing of CS4 as mentioned above. We further measured the relative dielectric constant ($\epsilon_r$) of neat films of SMAs. As revealed in Figure 2f, CS4 possesses a higher average $\epsilon_r$ (3.10) versus CH3 (2.43). This increase aligns directly with CS4's larger dipole moment and more compact intermolecular $\pi$–$\pi$ stackings.[46,47]

The above studies confirm the significant impact of the sulfur-bridged phenyl group on the intrinsic physicochemical properties of NFAs. Subsequently, the wide-bandgap polymer D18[48] and other polymer donors, such as PM6 and D18-Cl (Figures S5 and S6, Table S4, Supporting Information) were blended with NFAs to fabricate OSCs with a conventional device architecture (**Figure 3**a). We use 3-BPIC-F as hole transport layer reported in our previous work.[49] The chemical structure of 3-BPIC-F and its energy level alignment have been provided in Figure S7 and Table S5 (Supporting Information), respectively. Figure 3b presents the current density–voltage (*J*–*V*) characteristics of the optimized organic solar cells (OSCs), with key photovoltaic parameters detailed in **Table 1**. The device based on the D18:CH3 blend achieved a power conversion efficiency (PCE) of 17.92%, accompanied by an open-circuit voltage ($V_{OC}$) of 0.935 V, a short-circuit current density ($J_{SC}$) of 24.30 mA $cm^{-2}$, and a fill factor (FF) of 77.78%. In comparison, the D18:CS4-based device demonstrated a PCE of 18.57%, with a slightly higher $V_{OC}$ of 0.940 V, a $J_{SC}$ of 24.12 mA $cm^{-2}$, and a much better FF of 81.94%. After introducing BTP-eC9 as the third component, the champion ternary device afforded an impressive PCE of 20.16%, with

**Table 1.** Summary of photovoltaic parameters for OSCs.

| Active layers[a)] | $V_{oc}$ [V] | $J_{sc}$ [mA cm$^{-2}$] | Cal. $J_{sc}$[b)] [mA cm$^{-2}$] | FF [%] | PCE [%] |
|---|---|---|---|---|---|
| D18:CH3 | 0.935 (0.933 ± 0.004) | 24.30 (24.50 ± 0.30) | 23.21 | 77.78 (78.17 ± 0.77) | 17.92 (17.75 ± 0.10) |
| D18:CS4 | 0.940 (0.932 ± 0.003) | 24.12 (24.62±0.31) | 23.06 | 81.94 (80.39 ± 0.84) | 18.57 (18.45 ± 0.09) |
| D18:CS4:eC9 | 0.874 (0.877 ± 0.004) | 28.65 (28.69 ± 0.22) | 27.36 | 80.55 (79.35 ± 0.63) | 20.16 (19.93 ± 0.14) |

[a)] Statistical parameters calculated from 10 individual devices (Table S6–S8, Supporting Information); [b)] $J_{SC}$ determined by integration of the EQE spectra.

a $V_{OC}$ of 0.874 V, a $J_{SC}$ of 28.65 mA cm$^{-2}$, and a prominent FF of 80.55%. A close correlation was observed between the current density values integrated from the external quantum efficiency (EQE) plots (Figure 3c) and those from the *J*–*V* characterization, indicating minimal measurement error and consistent device performance. We have measured the photoluminescence quantum yield (PLQY) of CH3 and CS4 (Figure S8, Supporting Information). CS4 possesses a significantly higher PLQY value (9.92%) compared to CS3 (4.37%). A higher PLQY of CS4 acceptor may lead to an increased open-circuit voltage ($V_{OC}$) by reducing non-radiative recombination assisted by defects.[50]

In addition to PCE, the long-term operational stability of OSCs is critical for their widespread commercial applications. As shown in Figure 3d, all three devices exhibit good storage stability, maintaining above 83% of their initial PCEs after 2700 h in a glovebox under nitrogen. Considering that the devices can be affected by external factors such as light and heat during usage, the thermal/photo stability was further evaluated. Under the pressure of 65 °C, the PCE of the D18:CH3-based device dropped to 80% after 800 h (Figure 3e). In sharp contrast, the D18:CS4-based device afforded a $T_{80}$ lifetime of 1200 h, while the D18:CS4:BTP-eC9-based ternary device can retain 80% of their initial PCE after continuous heating for 2500 h. Under continuous light illumination (AM 1.5G, 100 mW cm$^{-2}$), the D18:CH3-based device only had a $T_{80}$ lifetime of 50 h. By contrast, D18:CS4-based devices possess a reduced PCE loss on this timescale and exhibit a $T_{80}$ lifetime of 550 h. Moreover, the D18:CS4:BTP-eC9-based ternary device afforded a $T_{80}$ lifetime of 710 h (Figure 3f). The increased device stability is consistent with the tighter molecular packing of CS4 and also closely related to the optimized film morphology discussed below.

The devices based on D18:CS4:eC9 demonstrated the highest exciton dissociation probability ($\eta_{diss}$) of 98.09% and the most efficient charge collection ($\eta_{coll}$) of 89.84%. In comparison, the D18:CS4-based devices showed values of 96.37% ($\eta_{diss}$) and 89.23% ($\eta_{coll}$), while the D18:CH3-based devices exhibited the lowest efficiencies, with a $\eta_{diss}$ of 96.05% and a $\eta_{coll}$ of 87.41% (Figure S9, Supporting Information).[51] Figure S10 (Supporting Information) shows the little bimolecular recombination loss for all three OSCs,[52] while Figure S11 (Supporting Information) displayed gradually suppressed trap-assisted recombination.[53] In addition, transient photovoltage (TPV) measurement afforded the charge lifetimes of 61.68, 80.33 and 98.73 µs for D18:CH3-, D18:CS4- and D18:CS4:eC9-based OSCs (Figure S12, Supporting Information), respectively, in good accordance with the tendency of trap-assisted recombination. Transient photocurrent (TPC) decay characterization (Figure S13, Supporting Information) yielded charge extraction times of 0.62, 0.50 and 0.41 µs for the D18:CH3, D18:CS4 and D18:CS4:eC9 blends, respectively. The stepwise decreased extraction time suggests the optimized charge transport, which agrees well with the enlarged and more balanced charge mobility from D18:CH3, D18:CS4 to D18:CS4:eC9 (Figure S14, Supporting Information).

The improvement of PCEs and FFs is largely derived from the optimized D/A blended morphology. As displayed by the atomic force microscopy based infrared spectroscopy (AFM-IR), all three blends were characteristic of a relatively smooth film surface (Figure S15, Supporting Information). Moreover, it is obvious that a well-defined nanofibrillar architecture is formed in both D18:CS4 and D18:CS4:eC9 blends, characterized by highly distinct phase boundaries between the donor and acceptor components (**Figure 4a**). The fiber sizes of D18:CH3, D18:CS4 and D18:CS4:eC9 gradually decreased from 15.3, 14.8 to 13.7 nm, respectively, which may contribute to the appropriate molecular crystallinity for D18:CS4:eC9 (Figure 4b; Figure S16, Supporting Information). The observed reduction in nanofiber size for CS4, compared to CH3, is likely attributable to its superior miscibility with the D18 polymer donor, as evidenced by a lower Flory–Huggins interaction parameter ($\chi$ values of 0.039 for CS4 vs 0.188 for CH3, Figure S17 and Table S9, Supporting Information).[54–55] This enhanced compatibility promotes a more homogeneous and finer phase-separated morphology in the blend. The improved intermixing also favors stronger interfacial contact, thereby enabling more efficient charge extraction and contributing to enhanced device performance.

GIWAXS was further used to investigate the molecular packing behavior in blend films. As illustrated in Figure 4c,d, the D18:CS4 blend maintains a preferential face-on molecular orientation, which facilitates efficient vertical charge transport. This blend also exhibits a reduced $\pi$–$\pi$ stacking distance of 3.63 Å and an increased CCL of 22.25 Å, compared to 3.88 and 20.86 Å, respectively, for the D18:CH3 blend. These results suggest enhanced molecular order and tighter packing in the D18:CS4 system (Table S10, Supporting Information). The presence or absence of sulfur-bridged phenyl group on the central unit induces distinct molecular ordering patterns, showing its function as a molecular stacking regulator. After introducing a third component, a reduced $\pi$–$\pi$ stacking distance of 3.53 Å and an enlarged CCL of 24.36 Å were further achieved. The favorable molecular packing behavior in ternary blend films agrees with its significantly improved device performance.

## 3. Conclusion

To effectively tune the molecular stacking characters of acceptors without affecting the molecular energy levels greatly, a

 

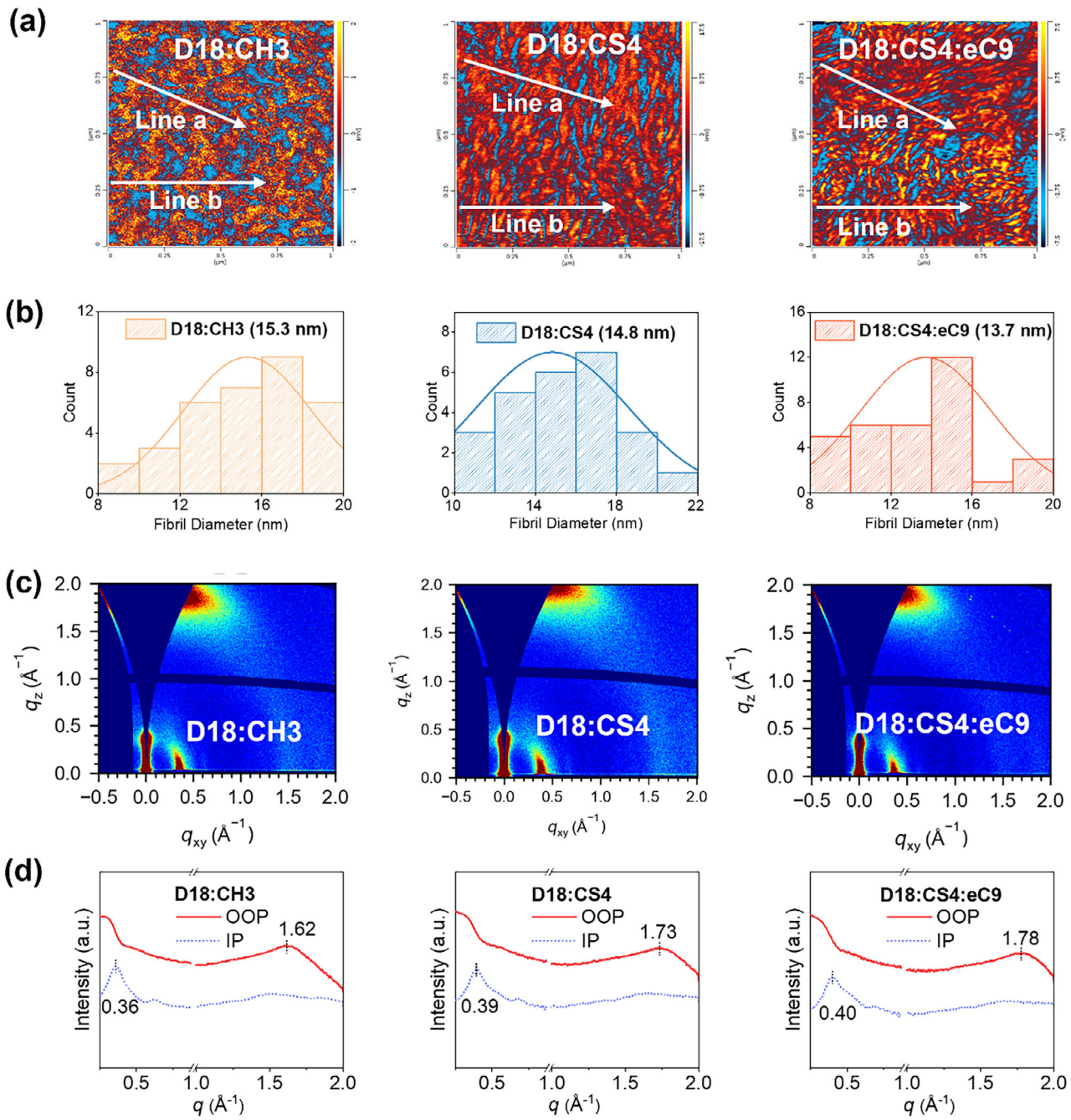


**Figure 4.** a) AFM-IR chemical mapping of the blend film, with donor and acceptor phases pseudocolored in blue and red, respectively. b) Corresponding statistical distribution of domain sizes. c) 2D GIWAXS patterns of blended films. d) In-plane (IP) and out-of-plane (OOP) line-cut profiles extracted from 2D GIWAXS.

sulfur-bridged and chlorinated phenyl group perpendicular to the central planes was explored as a molecular stacking regulator. Benefitting from the positive regulation of molecular topological structure, the newly constructed acceptor of CS4 exhibits tighter molecular packing, more balanced charge mobility, superior phase separation and reduced energetic disorder compared to its counterpart, CH3. Consequently, binary organic solar cells based on D18:CS4 achieved a higher PCE of 18.57%, outperforming the control device of D18:CH3 (17.81%). Remarkably, the ternary device D18:CS4:BTP-eC9 delivered a champion PCE of 20.16%. Compared to D18:CH3, D18:CS4 and ternary devices show superior stability. Under thermal stress at 65 °C, $T_{80}$ reaches 1200 h for D18:CS4 and 2500 h for ternary. Under continuous light illumination, $T_{80}$ is 550 and 710 h, respectively. Our work demonstrates that a delicately designed building block perpendicular to the central planes of acceptors could act as an effective and positive molecular stacking regulator. These insights are valuable to clarify the relationship between material

structure and molecular stacking and provide innovative strategies for high-performance OSCs.

## Supporting Information

Supporting Information is available from the Wiley Online Library or from the author.

## Acknowledgements

The authors gratefully acknowledged the financial support from the Ministry of Science and Technology of the People's Republic of China, National Key R&D Program of China (2022YFB4200400), the National Natural Science Foundation of China (22361132530; 52025033; 52373189; 22479081; 22309090), the Natural Science Foundation of Tianjin (23JCZDJC01160).

## Conflict of Interest

The authors declare no conflict of interest.

## Author Contributions

S.L. and Z.X. contributed equally to this work.

## Data Availability Statement

The data that support the findings of this study are available from the corresponding author upon reasonable request.

## Keywords

central unit, molecular stacking, non-fullerene acceptors, organic solar cells, sulfur-bridged

Received: September 25, 2025
Revised: October 22, 2025
Published online:

[1] S. R. Forrest, *Nat. Rev. Mater.* **2023**, *8*, 186.
[2] H. Li, S. Zeng, H. Zhao, Q. Liu, T. Xue, S. Liu, H. Li, L. Hu, E. Zhou, M. Khumalo, X. Hu, Y. Chen, *Adv. Mater.* **2025**, *37*, 2507761.
[3] L. Meng, Y. Zhang, X. Wan, C. Li, X. Zhang, Y. Wang, X. Ke, Z. Xiao, L. Ding, R. Xia, H.-L. Yip, Y. Cao, Y. Chen, *Science* **2018**, *361*, 1094.
[4] S. Li, Z. Li, X. Wan, Y. Chen, *eScience* **2023**, *3*, 100085.
[5] W. Song, K. Yu, E. Zhou, L. Xie, L. Hong, J. Ge, J. Zhang, X. Zhang, R. Peng, Z. Ge, *Adv. Funct. Mater.* **2021**, *31*, 2102694.
[6] Y. Li, X. Huang, H. K. M. Sheriff, S. R. Forrest, *Nat. Rev. Mater.* **2022**, *8*, 186.
[7] H. Li, J. Le, H. Tan, L. Hu, X. Li, K. Zhang, S. Zeng, Q. Liu, M. Zhang, L. Shi, Z. Cai, S. Liu, H. Li, L. Ye, X. Hu, Y. Chen, *Adv. Mater.* **2025**, *37*, 2411989.
[8] J. Yu, J. Pu, D. Xie, Z. Ai, Y. Lang, M. Cao, C. Duan, L. Lu, G. Li, *Nat. Commun.* **2025**, *16*, 7421.
[9] J. Ding, H. Mou, H. Chen, J. Xu, W. Sun, J. Zhu, Y. Wang, Y. Huang, Y. Li, Y. Li, *Adv. Mater.* **2025**, *37*, 2420439.
[10] S. Yang, X. Huang, Y. Cho, S. Koo, Y. Ouyang, Z. Sun, S. Jeong, T. L. H. Mai, W. Kim, L. Zhong, S. Chen, C. Zhang, H. S. Lee, S. J. Yoon, L. Chen, C. Yang, *Angew. Chem., Int. Ed.* **2025**, *64*, 202424287.
[11] J. Yuan, Y. Zhang, L. Zhou, G. Zhang, H.-L. Yip, T.-K. Lau, X. Lu, C. Zhu, H. Peng, P. A. Johnson, M. Leclerc, Y. Cao, J. Ulanski, Y. Li, Y. Zou, *Joule* **2019**, *3*, 1140.
[12] C. Li, J. Zhou, J. Song, J. Xu, H. Zhang, X. Zhang, J. Guo, L. Zhu, D. Wei, G. Han, J. Min, Y. Zhang, Z. Xie, Y. Yi, H. Yan, F. Gao, F. Liu, Y. Sun, *Nat. Energy* **2021**, *6*, 605.
[13] Y. Cui, H. Yao, J. Zhang, K. Xian, T. Zhang, L. Hong, Y. Wang, Y. Xu, K. Ma, C. An, C. He, Z. Wei, F. Gao, J. Hou, *Adv. Mater.* **2020**, *32*, 1908205.
[14] S. Guan, Y. Li, C. Xu, N. Yin, C. Xu, C. Wang, M. Wang, Y. Xu, Q. Chen, D. Wang, L. Zuo, H. Chen, *Adv. Mater.* **2024**, *36*, 2400342.
[15] L. Wang, C. Chen, Z. Gan, C. Liu, C. Guo, W. Xia, W. Sun, J. Cheng, Y. Sun, J. Zhou, Z. Chen, D. Liu, W. Li, T. Wang, *J. Energy Chem.* **2024**, *96*, 345.
[16] C. Li, Y. Cai, P. Hu, T. Liu, L. Zhu, R. Zeng, F. Han, M. Zhang, M. Zhang, J. Lv, Y. Ma, D. Han, M. Zhang, Q. Lin, J. Xu, N. Yu, J. Qiao, J. Wang, X. Zhang, J. Xia, Z. Tang, L. Ye, X. Li, Z. Xu, X. Hao, Q. Peng, F. Liu, L. Guo, H. Huang, *Nat. Mater.* **2025**, *24*, 1626.
[17] Z. Chen, S. Zhang, T. Zhang, J. Dai, Y. Yu, H. Li, X. Hao, J. Hou, *Joule* **2024**, *8*, 1723.
[18] Z. Wu, C. Sun, S. Dong, X.-F. Jiang, S. Wu, H. Wu, H.-L. Yip, F. Huang, Y. Cao, *J. Am. Chem. Soc* **2016**, *138*, 2004.
[19] J. Deng, W. Li, R. Zeng, J. Song, S. Tan, L. Kan, Z. Qin, Y. Zhao, F. Liu, Y. Sun, *Adv. Mater.* **2025**, *37*, 2501243.
[20] M. Zhang, L. Zhu, J. Yan, X. Xue, Z. Wang, F. Eisner, G. Zhou, R. Zeng, L. Kan, L. Wu, W. Zhong, A. Zhang, F. Han, J. Song, N. Hartmann, Z. Zhou, H. Jing, H. Zhu, S. Xu, J. Nelson, Y. Zhang, F. Liu, *Joule* **2025**, *9*, 101851.
[21] R. Zhang, H. Chen, T. Wang, L. Kobera, L. He, Y. Huang, J. Ding, B. Zhang, A. Khasbaatar, S. Nanayakkara, J. Zheng, W. Chen, Y. Diao, S. Abbrent, J. Brus, A. H. Coffey, C. Zhu, H. Liu, X. Lu, Q. Jiang, V. Coropceanu, J.-L. Brédas, Y. Li, Y. Li, F. Gao, *Nat. Energy* **2025**, *10*, 124.
[22] H. Chen, Y. Huang, R. Zhang, H. Mou, J. Ding, J. Zhou, Z. Wang, H. Li, W. Chen, J. Zhu, Q. Cheng, H. Gu, X. Wu, T. Zhang, Y. Wang, H. Zhu, Z. Xie, F. Gao, Y. Li, Y. Li, *Nat. Mater.* **2025**, *24*, 444.
[23] L. Wang, C. Chen, Y. Fu, C. Guo, D. Li, J. Cheng, W. Sun, Z. Gan, Y. Sun, B. Zhou, C. Liu, D. Liu, W. Li, T. Wang, *Nat. Energy* **2024**, *9*, 208.
[24] C. Li, J. Song, H. Lai, H. Zhang, R. Zhou, J. Xu, H. Huang, L. Liu, J. Gao, Y. Li, M. H. Jee, Z. Zheng, S. Liu, J. Yan, X.-K. Chen, Z. Tang, C. Zhang, H. Y. Woo, F. He, F. Gao, H. Yan, Y. Sun, *Nat. Mater.* **2025**, *24*, 433.
[25] X. Song, B. Zhang, X. Liu, L. Mei, H. Li, S. Yin, X. Zhou, H. Chen, Y. Lin, W. Zhu, X.-K. Chen, *Adv. Mater.* **2025**, *37*, 2418393.
[26] B. Fan, H. Gao, L. Yu, R. Li, L. Wang, W. Zhong, Y. Wang, W. Jiang, H. Fu, T. Chen, B. Kan, S. W. Tsang, A. K. Y. Jen, *Angew. Chem., Int. Ed.* **2024**, *64*, 202418439.
[27] L. Wang, C. Chen, Z. Gan, J. Cheng, Y. Sun, J. Zhou, W. Xia, D. Liu, W. Li, T. Wang, *Adv. Mater.* **2025**, *37*, 2419923.
[28] J. Dong, Y. Li, C. Liao, X. Xu, L. Yu, R. Li, Q. Peng, *Energy Environ. Sci.* **2025**, *18*, 4982.
[29] Y. Jiang, S. Sun, R. Xu, F. Liu, X. Miao, G. Ran, K. Liu, Y. Yi, W. Zhang, X. Zhu, *Nat. Energy* **2024**, *9*, 975.
[30] Y. Jiang, K. Liu, F. Liu, G. Ran, M. Wang, T. Zhang, R. Xu, H. Liu, W. Zhang, Z. Wei, Y. Cui, X. Lu, J. Hou, X. Zhu, *Adv. Mater.* **2025**, *37*, 2500282.
[31] L. Hu, J. Wang, F. Wang, G. Shen, H. Li, W. Li, Y. Jin, Z. Su, M. Du, J. Yao, Z. Yan, P. Cheng, D. Zhou, E. Zhou, Z. Li, *Adv. Funct. Mater.* **2025**, 20155.
[32] H. Tang, Z. Shen, Y. Shen, G. Yan, Y. Wang, Q. Han, L. Han, *Science* **2024**, *383*, 1236.
[33] Y. Li, X. Ru, M. Yang, Y. Zheng, S. Yin, C. Hong, F. Peng, M. Qu, C. Xue, J. Lu, L. Fang, C. Su, D. Chen, J. Xu, C. Yan, Z. Li, X. Xu, Z. Shao, *Nature* **2024**, *626*, 105.

 

[34] W. Wu, H. Gao, L. Jia, Y. Li, D. Zhang, H. Zhan, J. Xu, B. Li, Z. Geng, Y. Cheng, H. Tong, Y. Pan, J. Liu, Y. He, X. Xu, Z. Li, B. He, M. Zhou, L. Wang, C. Qin, *Science* **2025**, *389*, 195.
[35] Z. Fu, J.-W. Qiao, F.-Z. Cui, W.-Q. Zhang, L.-H. Wang, P. Lu, H. Yin, X.-Y. Du, W. Qin, X.-T. Hao, *Adv. Mater.* **2024**, *36*, 2313532.
[36] H. Lai, Y. Lang, Y. Luo, Z. Deng, Y. Wang, D. Qiu, R. Sun, G. Zhang, J. Wu, G. Li, F. He, *Adv. Energy Mater.* **2025**, 2406097.
[37] X. Wan, C. Li, M. Zhang, Y. Chen, *Chem. Soc. Rev.* **2020**, *49*, 2828.
[38] G. Wang, J. Wang, Y. Cui, Z. Chen, W. Wang, Y. Yu, T. Zhang, L. Ma, Y. Xiao, J. Qiao, Y. Xu, X.-T. Hao, J. Hou, *Angew. Chem., Int. Ed.* **2024**, *63*, 202401066.
[39] H. Yao, D. Qian, H. Zhang, Y. Qin, B. Xu, Y. Cui, R. Yu, F. Gao, J. Hou, *Chin. J. Chem.* **2018**, *36*, 491.
[40] Y. Lin, J. Wang, Z.-G. Zhang, H. Bai, Y. Li, D. Zhu, X. Zhan, *Adv. Mater.* **2015**, *27*, 1170.
[41] P. Li, X. Meng, K. Jin, Z. Xu, J. Zhang, L. Zhang, C. Niu, F. Tan, C. Yi, Z. Xiao, Y. Feng, G. W. Wang, L. Ding, *Carbon Energy* **2023**, *5*, 250.
[42] J. Guo, X. Cao, Z. Xu, T. He, X. Bi, Z. Yao, Y. Guo, G. Long, C. Li, X. Wan, Y. Chen, *J. Mater. Chem. A* **2025**, *13*, 356.
[43] Y.-B. Wang, C.-L. Tsai, Y.-J. Xue, B.-H. Jiang, H.-C. Lu, J.-C. Hong, Y.-C. Huang, K.-H. Huang, S.-Y. Chien, C.-P. Chen, Y.-J. Cheng, *Chem. Sci.* **2025**, *16*, 3259.
[44] P. Müller-Buschbaum, *Adv. Mater.* **2014**, *26*, 7692.
[45] Z. Wang, Y. Zhang, J. Zhang, Z. Wei, W. Ma, *Adv. Energy Mater.* **2016**, *6*, 1502456.
[46] Z. Fu, X. Zhang, H. Zhang, Y. Li, H. Zhou, Y. Zhang, *Chin. J. Chem.* **2021**, *39*, 381.
[47] X. Zhang, C. Li, J. Xu, R. Wang, J. Song, H. Zhang, Y. Li, Y.-N. Jing, S. Li, G. Wu, J. Zhou, X. Li, Y. Zhang, X. Li, J. Zhang, C. Zhang, H. Zhou, Y. Sun, Y. Zhang, *Joule* **2022**, *6*, 444.
[48] Q. Liu, Y. Jiang, K. Jin, J. Qin, J. Xu, W. Li, J. Xiong, J. Liu, Z. Xiao, K. Sun, S. Yang, X. Zhang, L. Ding, *Sci. Bull.* **2020**, *65*, 272.
[49] H. Liu, Y. Xin, Z. Suo, L. Yang, Y. Zou, X. Cao, Z. Hu, B. Kan, X. Wan, Y. Liu, Y. Chen, *J. Am. Chem. Soc.* **2024**, *146*, 14287.
[50] X.-K. Chen, D. Qian, Y. Wang, T. Kirchartz, W. Tress, H. Yao, J. Yuan, M. Hülsbeck, M. Zhang, Y. Zou, Y. Sun, Y. Li, J. Hou, O. Inganäs, V. Coropceanu, J.-L. Bredas, F. Gao, *Nat. Energy* **2021**, *6*, 799.
[51] A. K. K. Kyaw, D. H. Wang, C. Luo, Y. Cao, T.-Q. Nguyen, G. C. Bazan, A. J. Heeger, *Adv. Energy Mater.* **2014**, *4*, 1301469.
[52] P. Schilinsky, C. Waldauf, C. J. Brabec, *Appl. Phys. Lett.* **2002**, *81*, 3885.
[53] Y. Sun, L. Nian, Y. Kan, Y. Ren, Z. Chen, L. Zhu, M. Zhang, H. Yin, H. Xu, J. Li, X. Hao, F. Liu, K. Gao, Y. Li, *Joule* **2022**, *6*, 2835.
[54] S. Nilsson, A. Bernasik, A. Budkowski, E. Moons, *Macromolecules* **2007**, *40*, 8291.
[55] J. Comyn, *Int. J. Adhes. Adhes.* **1992**, *12*, 145.